ACS APPLIED MATERIALS & INTERFACES

Research Article

www.acsami.org

Aqueous Solution Synthesis of Pt–M (M = Fe, Co, Ni) Bimetallic Nanoparticles and Their Catalysis for the Hydrolytic Dehydrogenation of Ammonia Borane

Shuai Wang, Duo Zhang, Yanyun Ma,* Hui Zhang, Jing Gao, Yuting Nie, and Xuhui Sun*

Institute of Functional Nano and Soft Materials (FUNSOM), Jiangsu Key Laboratory for Carbon-Based Functional Materials and Devices, and Collaborative Innovation Center of Suzhou Nano Science and Technology, Soochow University, Suzhou, Jiangsu 215123, People's Republic of China

Supporting Information

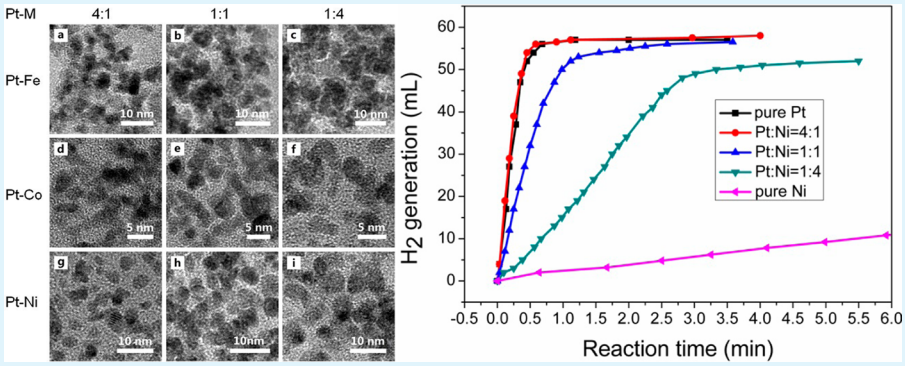

ABSTRACT: Platinum-based bimetallic nanocatalysts have attracted much attention due to their high-efficiency catalytic performance in energy-related applications such as fuel cell and hydrogen storage, for example, the hydrolytic dehydrogenation of ammonia borane (AB). In this work, a simple and green method has been demonstrated to successfully prepare Pt–M (M = Fe, Co, Ni) NPs with tunable composition (nominal Pt/M atomic ratios of 4:1, 1:1, and 1:4) in aqueous solution under mild conditions. All Pt–M NPs with a small size of 3–5 nm show a Pt *fcc* structure, suggesting the bimetallic formation (alloy and/or partial core–shell), examined by transmission electron microscopy (TEM), X-ray diffraction (XRD), and X-ray absorption fine structure (XAFS) analysis. The catalytic activities of Pt–M NPs in the hydrolytic dehydrogenation of AB reveal that Pt–Ni NPs with a ratio of 4:1 show the best catalytic activity and even better than that of pure Pt NPs when normalized to Pt molar amount. The Ni oxidation state in Pt–Ni NPs has been suggested to be responsible for the corresponding catalytic activity for hydrolytic dehydrogenation of AB by XAFS study. This strategy for the synthesis of Pt–M NPs is simple and environmentally benign in aqueous solution with the potential for scale-up preparation and the *in situ* catalytic reaction.

KEYWORDS: *bimetallic, nanoparticles, hydrolytic dehydrogenation, ammonia borane, XAFS*

INTRODUCTION

Platinum (Pt)-based nanomaterials have been widely used as the most effective catalyst in various fields such as fuel cell, battery, petrochemical, pharmaceutical, hydrogen-storage, and other chemical conversion reactions.[1−6] Unfortunately, the cost of Pt is extremely high due to its rarity in the earth and the incessantly growing demand, which is the biggest challenge for its wide applications, particularly, in fuel cell and automobile industries.[1,7] To date there are three main strategies to reduce the usage of Pt: (i) drastically improving the activities of a Pt-based catalysts via tuning the size, the morphology, the surface structure (or crystal plane) of Pt nanoparticles (NPs) to maximize the specific activity;[8−11] (ii) developing Pt-based multimetallic nanomaterials (alloy, core–shell, intermetallic) to partly replace Pt and thus obtain the same or even better catalytic activity;[12−16] (iii) developing non-Pt catalysts to achieve the complete replacement of Pt by less expensive metals.[17−21] Among these strategies, Pt–M (M = Fe, Co, Ni) bimetallic nanomaterials show a promising future due to specific activity better than that of pure Pt attributed to a synergistic effect between Pt and M.[22−27] There are many studies on successful synthesis of Pt–M bimetallic NPs with controllable size, shape, and composition.[28−33] However, most of Pt–M bimetallic catalysts were synthesized in the presence of surfactant and in the organic phase. Even though this approach shows some advantages of small size, well-defined shape, and good uniformity of the products, it has some disadvantages such as high reaction temperature, complicated operation, high cost, environmental pollution, and difficult removal of the organic surfactant. Therefore, it would be useful

Received: April 17, 2014
Accepted: July 24, 2014
Published: July 24, 2014

to achieve the synthesis of Pt−M bimetallic NPs in a green, simple, and low-cost strategy such as in aqueous solution and under mild conditions, by which the catalysts could be directly applied in the catalytic reaction without any treatment of washing and centrifugation. These superiorities cause the controlled synthesis of Pt−M bimetallic NPs in aqueous phase to have great competitiveness in liquid-phase catalysis, in particularly, in the field of hydrogen storage and generation.[34,35]

Ammonia borane (AB, NH_3BH_3) is one of the most attractive candidates for chemical hydrogen-storage application due to its high hydrogen content of 19.6 wt % which exceeds that of gasoline.[36−38] For the hydrolysis of AB, Pt-based catalysts, such as Pt/C, PtO_2, and K_2PtCl_4, have been reported to show the highest activity among all of the various catalysts.[39] In order to achieve the practical application of the Pt catalyst, however, there is still a challenge for the development of an efficient and economical catalyst to further decrease the Pt amount and improve the kinetic properties such as the release rate of hydrogen under mild conditions.

In this work, a simple, convenient, and green method has been employed to prepare Pt−M (M = Fe, Co, Ni) NPs in aqueous solution under mild conditions (ambient temperature), and a series of Pt−M (M = Fe, Co, Ni) NPs with controllable composition have been successfully synthesized and applied in the hydrolysis of AB. The Pt−Ni NPs (Pt:Ni = 4:1) show the highest hydrogen-release rate in all Pt−M samples when normalized to the Pt molar amount, which is even higher than that of pure Pt NPs prepared under the same conditions with the same total-mole concentration of metals. On the basis of the XAFS analysis of Pt L_3-edge and Ni K-edge, we found that the degree of disorder of Pt−M NPs increased with the increase of Ni content, and the best catalytic activity of Pt−Ni NPs (Pt:Ni = 4:1) could be attributed to the combined effect of Pt disorder and less oxidation of Ni on the surface. The strategy for synthesis of Pt−M bimetallic NPs in aqueous solution also has a potential to be developed on the scale-up preparation and the application of *in situ* catalytic reaction, which makes it more effective and useful in industry. Moreover, this method could be extended to the synthesis of other multimetallic nanostructures.

EXPERIMENTAL SECTION

1. Preparation of Pt−M (M = Fe, Co, Ni) NPs. In a typical experiment, 1 mL of 40 mM metallic precursor ($FeCl_2$, $CoCl_2$, or $NiCl_2$), 1 mL of 40 mM H_2PtCl_6 and 20 mL of 1 wt % polyvinylpyrrolidone (PVP) were mixed in a 100 mL beaker under stirring. After 5 min, 3 mL of 80 mM $NaBH_4$ (freshly prepared) was quickly injected into the solution under stirring. In order to remove excess $NaBH_4$, the beaker was slightly shaken until no obvious tiny bubbles were observed in the beaker. The product of Pt−M (1:1) NPs in a suspension liquid could be directly used for the hydrolytic dehydrogenation of AB without further treatment. Keeping the total metal molar amount constant, we can easily obtain Pt−M NPs with nominal Pt−M atomic ratios of 4:1, 1:1, 1:4, respectively, by adjusting the relative amount of M precursors and H_2PtCl_6. For example, 1.6 mL H_2PtCl_6 and 0.4 mL $NiCl_2$ were used as the precursors in the preparation of Pt−Ni NPs with an atomic ratio of approximate 4:1. Pure Pt NPs or pure M NPs with the same molar amount were also prepared in the same condition for comparison.

2. Characterization. The products were washed three times with H_2O and finally collected by centrifugation before a further characterization. The morphology and size of as-prepared nanoparticles were characterized by TEM (FEI Tecnai G^2 F20 S-TWIN) with an accelerating voltage of 200 kV, and equipped with an energy-dispersive X-ray (EDX) detector. TEM samples were prepared by loading the nanoparticles suspension solution onto a carbon-coated copper grid and then drying in air at ambient temperature. The crystallographic structure and composition of as-prepared nanoparticles were studied by X-ray powder diffraction (XRD). XRD patterns were recorded on a scintag PANalytical B.V. Empyrean powder diffractometer equipped with PIXcel3D detector, working with Cu Kα radiation (λ = 0.15406 nm). All XRD data were collected in the 2θ range from 10° to 90°. X-ray absorption fine structure (XAFS) spectra of as-prepared nanoparticles for Pt L_3-edge and M (M = Fe, Co, Ni) K-edge were collected on Beamline BL14W1 at the Shanghai Synchrotron Radiation Facility (SSRF). XAFS data were acquired in either transmission or fluorescence mode. XAFS spectra of standard samples, such as Ni foil and NiO powder, were obtained in the same conditions for comparison.

3. Catalytic Activity Measurement. At first, 5 mL of ammonia borane (AB, 0.5 wt %) was kept in a 50 mL three-neck round-bottom flask. The left and right necks were sealed with the rubber stoppers after adding AB. The middle neck was sealed with the rubber stopper which was connected to the gas-collection tube. The tube was inserted into a gas buret. Three mL freshly prepared Pt−M NPs (suspension liquid) were quickly injected into the flask through the left/right neck with an airtight syringe using the sharp needle. The reaction time was recorded from the appearance of the first bubble. The syringe was kept in the stopper until the experiment finished. The released gas was monitored using a gas buret. The reactions were carried out at room temperature under ambient atmosphere. The hydrolysis of NH_3BH_3 can be briefly expressed as follow:

$$NH_3BH_3 + 2H_2O \rightarrow NH_4^+ + BO_2^- + 3H_2$$

RESULTS AND DISCUSSION

The Pt−M nanoparticles (NPs) were synthesized by the coreduction of H_2PtCl_6 and metal precursors ($FeCl_2$, $CoCl_2$, or $NiCl_2$) with the reducing agent of $NaBH_4$ in the presence of polyvinylpyrrolidone (PVP) in aqueous solution. The composition of Pt−M NPs could be tuned by changing the corresponding mole ratio of H_2PtCl_6 and metal precursors while keeping the same total molar amount. The as-prepared nanoparticles were characterized by transmission electron microscopy (TEM) after washing and centrifugation. Figure 1 shows a series of TEM images of Pt−M NPs with different composition, indicating the formation of a sphere-like shaped Pt−M NPs in a slight aggregation with uniform size distribution. The size of a single Pt−M (M = Fe, Co, Ni) NP is 3−5 nm and increases slightly as the Pt−M ratio decreases due to the aggregation. The Pt−Fe NPs show the most serious aggregation as the Pt decreases. The size and shape of Pt-rich NPs is similar to that of pure Pt NPs synthesized under the same conditions (Supporting Information [SI], Figure S1). In addition, the atomic compositions of Pt−M (M = Fe, Co, Ni) NPs were determined by EDX analysis, approximately revealing the composition of the products. The average atomic compositions were obtained by averaging the EDX results of the corresponding samples in three random areas (SI, Table S1). The Pt−M ratios are around 4:1, 1:1, 1:4, respectively, which is similar to those of the Pt−M precursors. Although the actual ratios of Pt−M (in particular, the sample of Pt:Co = 1:4) in the final product do not exactly agree with those of the corresponding precursors, the trend of Pt−M ratio is always Pt-rich, Pt−M (equal ratio), M-rich, respectively. These results demonstrate that it is a simple, feasible, and generic method to prepare Pt−M bimetallic nanomaterals with variable atomic ratios in aqueous solution at ambient conditions.

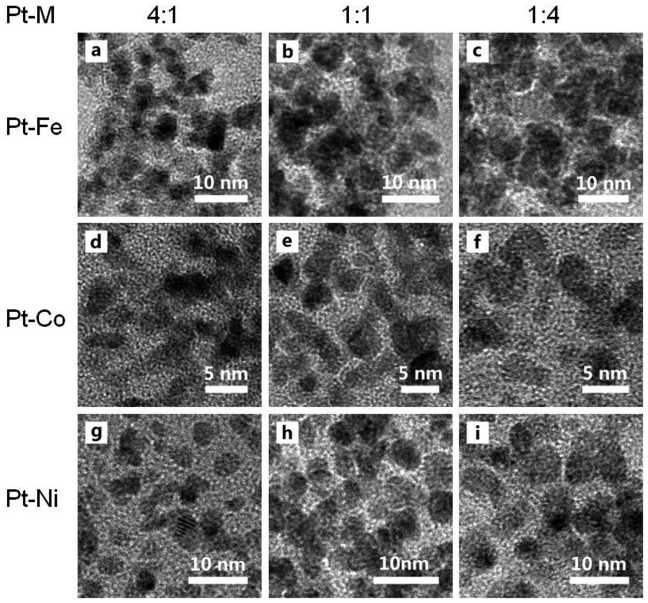

Figure 1. TEM images of Pt−M (M = Fe, Co, Ni) NPs synthesized with different atomic compositions by tuning the precursor-ratios of H_2PtCl_6 and metal precursors while keeping the same total metal molar amount: (a−c) Pt−Fe NPs, (d−f) Pt−Co NPs, (g−i) Pt−Ni NPs, (a, d, g) Pt:M = 4:1, (b, e, h) Pt:M = 1:1, (c, f, (i) Pt:M = 1:4. TEM image of pure Pt particles is shown in the SI Figure S1.

To further confirm the component and the crystal structure, Pt−M (M = Fe, Co, Ni) NPs with different composition ratios were characterized with powder X-ray diffraction (XRD), respectively (Figure 2). The XRD pattern of pure Pt NPs is indexed to a face-centered-cubic (*fcc*) structure of Pt (Figure 2c, purple curve). All main peaks of Pt−M NPs are very similar to those of Pt without the obvious feature peak of pure M, indicating that the products are not the mixtures of Pt and M, but bimetallic nanoparticles. The main diffraction peaks are much broader due to the nano size effect (3−5 nm) and the crystal defects due to the incorporation of M. The mean size of Pt NPs (4.1 nm) is deduced by the Scherrer equation, which agrees well with the corresponding TEM result (3−5 nm in Figure S1 in the SI). Compared to pure Pt NPs, the two main peaks of Pt−Fe NPs and Pt−Co NPs at low 2θ, which can be indexed to Pt (111) and Pt (200), do not show an obvious shift. The other two peaks (Pt (220) and Pt (311)) at high 2θ show a slight right-shift. It is worth noting that all diffraction peaks of Pt−Ni NPs show regular right-shifts to higher 2θ. Particularly, the degree of right-shift increases gradually along with the increase of Ni composition. For example, the Pt (111) diffractions of the three Pt−Ni samples are 40.26° for Pt−Ni (4:1) NPs, 40.67° for Pt−Ni (1:1) NPs, and 41.23° for Pt−Ni (1:4) NPs. These observed shifts are related to the change in atomic composition based on Vegard's law, that is, the peak positions change monotonically from low angle for Pt-rich NPs to high angle for Ni-rich NPs. The lattice parameters of the unit cells for Pt−Ni (4:1), Pt−Ni (1:1), and Pt−Ni (1:4) are 3.8787 ± 0.0029, 3.8583 ± 0.0050, and 3.8148 ± 0.0200, respectively, calculated on the basis of a NiPt alloy with a = 3.823 Å (JCPDS no. 65-2797). It shows a gradual shrinkage as the Ni content increases. Meanwhile, the peak intensities decrease with the increase of M content due to the decrease of Pt content and the increase of crystalline defects.

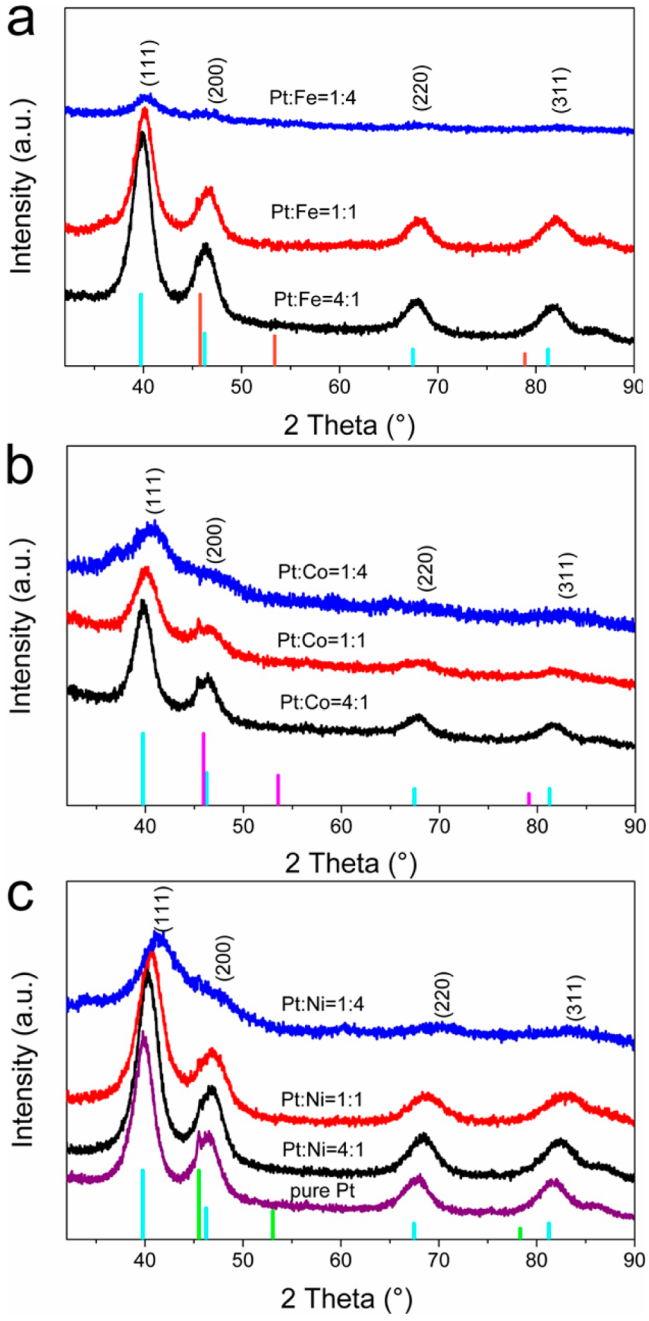

Figure 2. XRD patterns of pure Pt NPs and Pt−M (M = Fe, Co, Ni) NPs with different atomic ratios. Cyan bars: JCPDS no. 01-070-2431 (Pt); red bars in (a): no. 01-088-2324 (Fe); purple bars in (b): no.01-088-2325 (Co); green bars in (c): no. 01-088-2326 (Ni).

Ammonia borane (0.5 wt %, 5 mL) can be catalytically hydrolyzed by freshly prepared pure Pt NPs and Pt−M (M = Fe, Co, Ni) NPs with different composition, respectively. The comparison experiments of pure M NPs were also carried out under the same conditions. The generated hydrogen gas was measured volumetrically. Figure 3 shows the plots of the amount of hydrogen released during the hydrolytic dehydrogenation process with the freshly prepared Pt−M NPs. Clearly, Pt−Ni NPs show a higher H_2-release rate than Pt−Co and Pt−Fe NPs. The complete hydrolysis of AB finished in 0.75 min for Pt−Ni (4:1) NPs, 1.2 min for Pt−Ni (1:1) NPs, and 3 min for Pt−Ni (1:4) NPs (Figure 3a). For Pt−Co NPs, the hydrolysis of AB completely finished in approximately 1.5, 1.5, and 4 min

dx.doi.org/10.1021/am502335j | ACS Appl. Mater. Interfaces 2014, 6, 12429−12435

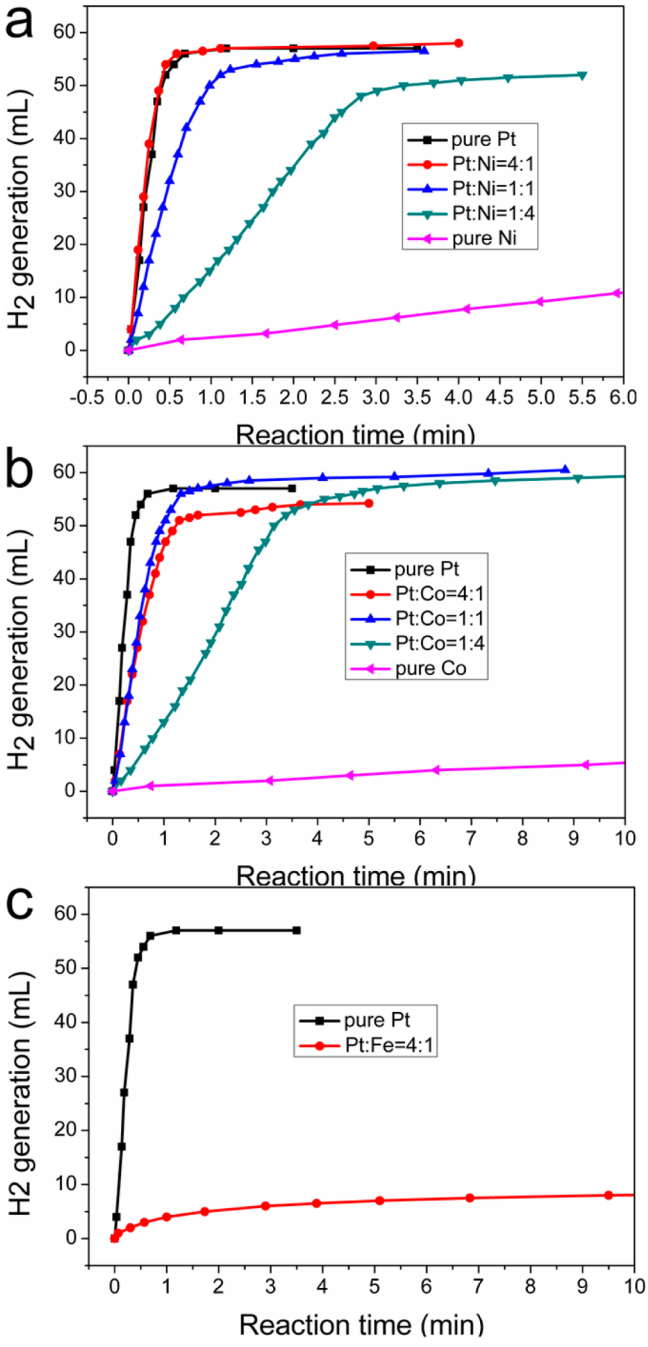

Figure 3. Hydrogen evolution of hydrolysis of AB aqueous solution (0.5 wt %, 5 mL) catalyzed by pure Pt NPs, pure M NPs, and Pt−M NPs with different ratios under ambient atmosphere: (a) Pt−Ni NPs, (b) Pt−Co NPs, (c) Pt−Fe NPs. The mole amount of total metal (Pt + M) in each catalyst is kept constant.

at Pt−Co ratios of 4:1, 1:1, and 1:4, respectively, which is slower than that of pure Pt NPs (about 0.75 min, Figure 3b). However, the Pt−Fe (4:1) NPs have little effect on the hydrolysis of AB even after 14 min (Figure 3c). In addition, it is obvious that Pt-based NPs show a much better catalyst activity than that of pure Ni or Co NPs (prepared under the same conditions) in the hydrolysis of AB, and less than one-fifth of the total hydrogen is released in around 6 min for pure Ni NPs. The theoretical H_2-release amount of 5 mL, 0.5 wt % AB at 25 °C at standard atmospheric pressure should be 59.5 mL. Pure Pt NPs, Pt−Ni (4:1 and 1:1) NPs and Pt−Co (1:1 and 1:4) NPs can almost reach this theoretical value, which means the complete decomposition of AB. Meanwhile, it is noted that the Pt−Ni NPs (4:1) show a similar H_2-release rate and amount compared to the pure Pt NPs. Because Pt−Ni (4:1) and Pt NPs were prepared with the same total metal molar amount, Pt−Ni (4:1) show the best catalytic activity in hydrolysis of AB when the H_2-release rate normalized to the Pt molar amount,[40] even better than that of pure Pt NPs as shown in Table 1. In addition, the effect of excess $NaBH_4$ (the reactant of H_2PtCl_6 in preparing Pt−M NPs) on the total H_2 release amount has been considered because the Pt−M suspension liquid is used in the hydrolytic dehydrogenation process immediately without any treatment such as centrifugation. To our knowledge, the obvious tiny bubbles can be easily observed when $NaBH_4$ aqueous solution is stirred or even static when it is hydrolyzed at room temperature. In our experiments, after the preparation of Pt or Pt−M catalysts, the beaker with suspension solution had been shaken for several minutes until there were no obvious tiny bubbles observed. Thus, the excess $NaBH_4$ had almost been hydrolyzed completely before adding the suspension into AB and the effect of any excess $NaBH_4$ on the measured total H_2 release is too small to significantly affect these experiments. This result demonstrates that the Pt−Ni NPs with appropriate composition might have a promising application in hydrogen storage because of the cutting of the Pt amount.

While the catalysis mechanism of Pt−M bimetallic NPs has been discussed widely, which could be ascribed to the synergistic effects of M and Pt such as the electronic effect and the geometric effect,[22−27] it is still very crucial and necessary to deeply reveal the essential effect of the electronic structure and the local structure of Pt−M NPs on the corresponding catalytic activity. The electronic structure and local structure of Pt−M NPs have been investigated by XAFS, which deals with the measurement and interpretation of absorption coefficient above a specific absorption edge, in this case, the Pt $L_{3,2}$-edge and M K-edge. XAFS spectroscopy, containing XANES (X-ray absorption near edge structure) and EXAFS (extended X-ray absorption fine structure), has been demonstrated as the most powerful tool to systematically study

Table 1. H_2 Release Rates for Pure Pt NPs, Pure Ni NPs and Pt−Ni NPs with Different Ratios under Ambient Atmosphere: H_2 Release Rate Based on Original H_2 Volume (second column), the One Normalized to Total Metal Molar Amount (Cat-M, third column), and the One Normalized to Pt Molar Amount (Cat-Pt, fourth column) at Ambient Condition, Respectively

catalysts	mL/min	(H_2) mol/(Cat-M)mol·min	(H_2) mol/(Cat-Pt)mol·min
pure Pt	115.5	492	492
Pt:Ni = 4:1	120.0	511	638
Pt:Ni = 1:1	50.0	213	426
Pt:Ni = 1:4	17.0	72	360
pure Ni	1.0	4.0	–

the composition and the structure of nanoparticles via showing valence state, bonding type, bond length, electronic structure, and so on. It also has been used for the structure study of Pt−M bimetallic nanomaterials.[41−45] The excitations in the near edge region in the vicinity of the threshold arise from the core to bound and quasi-bound unoccupied state dipole transitions. These features are the XANES, which probes densities of states and local symmetry. As the excitation energy increases, the photoelectron gains sufficient energy, leaving the absorbing atom. As the photoelectron travels away from the absorbing atom, it will be scattered by the neighboring atoms. Therefore, the constructive and destructive interference of these outgoing and backscattered waves produce oscillations in the absorption coefficient. These oscillations are the EXAFS, denoted $\chi(k)$, which contains information about the interatomic distance and the local dynamics of the system, $\chi(k) = \varphi(k)A(k)$, where $\varphi(k)$ is the phase (containing bond length and phase information) and $A(k)$ the amplitude (containing information about the backscattered atom, the bond length, the coordination number and the Debye−Waller factor - thermal mean square displacement of the interatomic distance). EXAFS is only sensitive to short-range order due to the short attenuation length of electrons. EXAFS can be readily analyzed using a Fourier transform technique, which separates the phase and the amplitude. The as-prepared pure Pt NPs, pure Ni NPs, and Pt−M (M = Fe, Co, Ni) NPs with different ratios were characterized by XAFS. Figure 4 shows the Pt L_3-edge and Ni K-edge XANES spectra of Pt−Ni NPs, respectively, along with Pt NPs, Ni NPs, Ni foil, and NiO as references. The strong absorption bands at both L_3 and L_2 X-ray absorption edges are called white lines. The intensity of white line for Pt L_3-edge is proportional to the unoccupied *d*-orbital of *d* group metals. In Figure 4a, the position and area of white line around 11568 eV for Pt−Ni NPs are similar to that of Pt NPs. The result reveals the predominantly metallic state of Pt in Pt−Ni NPs, which is consistent with the former XRD and TEM results and is further confirmed by the later EXAFS study. In contrast, the Ni K-edge XANES of Pt−Ni NPs exhibit apparently different features. Ni NPs and Pt−Ni (4:1) NPs show features similar to that of Ni foil, but the double-peak around 8350−8360 eV, which is characteristic of *fcc* metallic Ni, changes to a single peak as shown in Figure 4b, indicating that Ni was partially oxidized in the product. Furthermore, Pt−Ni (4:1) NPs have the weaker pre-edge feature of Ni at 8334 eV compared to those of Ni foil and Ni NPs, which suggests that Ni in Pt−Ni (4:1) NPs is slightly oxidized but still keeps its metallic feature. Yet Pt−Ni (1:1) NPs and Pt−Ni (1:4) NPs show features similar to those of NiO, which indicates the dominant oxidation state of Ni in the latter two Pt−Ni catalysts is +2. In addition, there is still a weak pre-edge feature left at 8334 eV in Pt−Ni (1:1) NPs, indicating that some metallic Ni exists in the form of the Ni oxidation state.[46] It could be concluded that the oxidation state of Ni in the Pt−Ni NPs increases with the increase of Ni content.

The local geometric structure of Pt and Ni atoms for Pt−Ni NPs can be obtained by simultaneously analyzing the corresponding EXAFS data (Figure 5). Magnitudes of Fourier transform (FT) to the EXAFS spectra at Pt L_3-edge (Figure 5a) show that the main peak position for Pt−Pt bond left-shifted from 2.82 to 2.70 Å with the increase of Ni content, indicating the lengths of Pt−Pt bond shrink at the insertion of Ni and disorder of the Pt nanostructures with small size.[47] Magnitudes of FT to the EXAFS spectra at Ni K-edge are shown in Figure

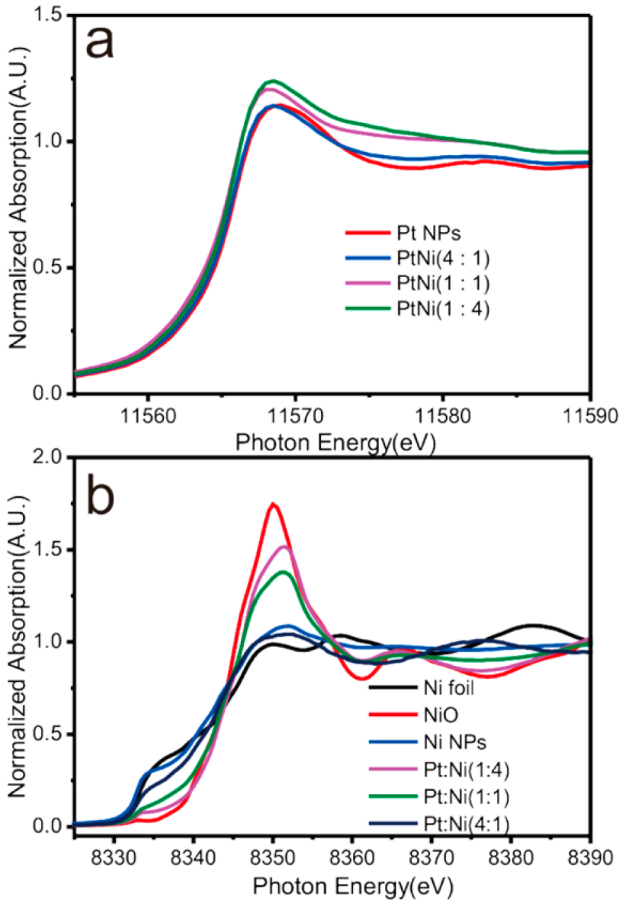

Figure 4. (a) Normalized absorption spectra at the Pt L_3-edge for the corresponding Pt−Ni catalysts with three different ratios and pure Pt NPs. (b) Normalized absorption spectra at the Ni K-edge for the corresponding Pt−Ni catalysts with three different ratios, pure Ni NPs, and references of Ni foil, Ni NPs, and NiO.

5b. It is obvious that Ni NPs and Pt−Ni (4:1) NPs show a single main peak at around 2.4 Å, having the features similar to that of Ni foil. In contrast, there are two main peaks for Pt−Ni (1:1) and Pt−Ni (1:4) NPs at about 1.8 and 3.0 Å, which are similar to those of the NiO standard sample. These two peaks show slight shifts in different degrees due to the content of Pt, and might be ascribed to Ni−O and Ni−O−Ni (or Ni−O−Pt) contribution,[41] respectively. The results imply that Ni in Pt−Ni (4:1) NPs shows more metallic features compared to Pt−Ni (1:1) and Pt−Ni (1:4) NPs, which agrees with XANES result and might be responsible for the best catalytic activity.

CONCLUSION

In this work, ratio-controllable Pt−M (M = Fe, Co, Ni) NPs have been synthesized by the coreduction of H_2PtCl_6 and metal precursors with $NaBH_4$ in the presence of polyvinylpyrrolidone (PVP) in aqueous solution at mild conditions. The products mainly display a Pt *fcc* structure with the indications for bimetallic formation (alloy and/or partial core−shell) via XRD and XAFS analysis. In addition, for the hydrolytic dehydrogenation of ammonia borane, both Pt−Ni (4:1, 1:1) NPs and Pt−Co (4:1, 1:1) NPs show a good catalytic activity. Among them, the Pt−Ni NPs with a ratio of 4:1 even exhibit the better H_2-release rate than that of pure Pt NPs prepared under the same conditions when normalized to Pt molar amount. XAFS (both XANES and EXAFS) study confirms the predominantly

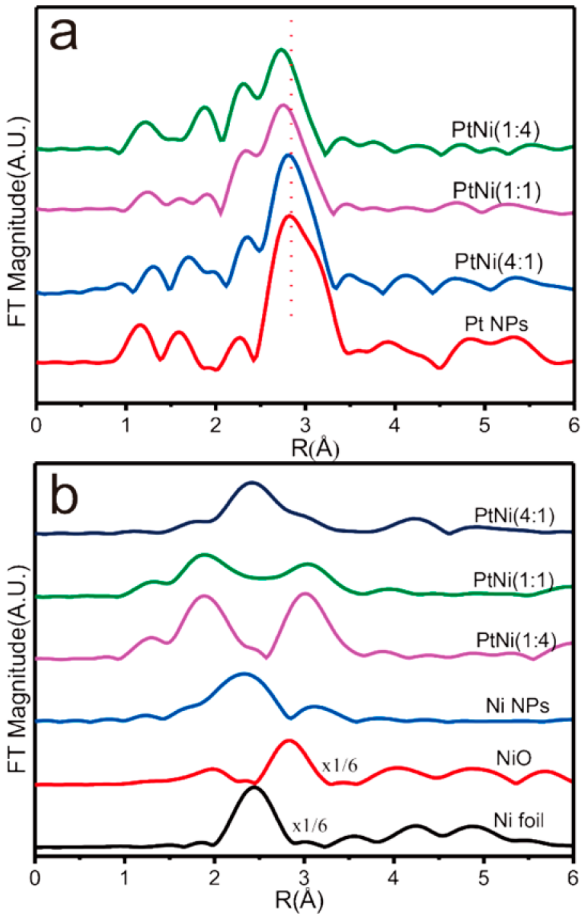

Figure 5. (a) Magnitude of k^3-weighted Fourier transform of Pt L_3-edge EXAFS for the corresponding Pt–Ni catalysts with three different ratios of Pt/Ni and reference of Pt NPs. (b) Magnitude of k^3-weighted Fourier transform of Ni K-edge EXAFS for the corresponding Pt–Ni catalysts with three different ratios of Pt/Ni and references of Ni NPs, Ni foil, and NiO powder.

metallic state of Pt in all Pt–Ni NPs and the higher degree of disorder in Pt–Ni NPs, which is consistent with the XRD and TEM results. The XAFS results demonstrate that metallic Ni is in Pt–Ni (4:1) NPs but higher oxidation state of Ni in Pt–Ni (1:1) NPs and Pt–Ni (1:4) NPs, which might be the essential reason for their different catalytic activities. This work provides a simple and environmentally benign method for the controllable synthesis of bimetallic nanoparticles in aqueous solution, which could be directly used in the in situ catalytic reaction without any treatment.

■ ASSOCIATED CONTENT

Ⓢ Supporting Information

TEM image of pure Pt NPs, EDX data for Pt–M (M = Fe, Co, Ni) NPs with different atomic ratios. This material is available free of charge via the Internet at http://pubs.acs.org.

■ AUTHOR INFORMATION

Corresponding Authors

*E-mail: mayanyun@suda.edu.cn. Fax: 86-512-65880820. Tel: 86-512-65884530.

*E-mail: xhsun@suda.edu.cn. Fax: 86-512-65880820. Tel: 86-512-65880943.

Notes

The authors declare no competing financial interest.

■ ACKNOWLEDGMENTS

The authors thank beamline BL14W1 (Shanghai Synchrotron Radiation Facility) for providing the beam time. The work was supported by the National Basic Research Program of China (973 Program) (Grant No. 2010CB934500), Natural Science Foundation of China (NSFC) (Grant No. 91333112, 21203130), the Priority Academic Program Development of Jiangsu Higher Education Institutions. This is also a project supported by the Fund for Innovative Research Teams of Jiangsu Higher Education Institutions.

■ REFERENCES

(1) Gasteiger, H. A.; Kocha, S. S.; Sompalli, B.; Wagner, F. T. Activity Benchmarks and Requirements for Pt, Pt-alloy, and Non-Pt Oxygen Reduction Catalysts for PEMFCs. *Appl. Catal., B* **2005**, *56*, 9–35.

(2) Lu, Y. C.; Xu, Z. C.; Gasteiger, H. A.; Chen, S.; Hamad-Schifferli, K.; Shao-Horn, Y. Platinum–Gold Nanoparticles: A Highly Active Bifunctional Electrocatalyst for Rechargeable Lithium–air Batteries. *J. Am. Chem. Soc.* **2010**, *132*, 12170–12171.

(3) Klajn, R.; Bishop, K. J. M.; Fialkowski, M.; Paszewski, M.; Campbell, C. J.; Gray, T. P.; Grzybowski, B. A. Plastic and Moldable Metals by Self-assembly of Sticky Nanoparticle Aggregates. *Science* **2007**, *316*, 261–264.

(4) Tao, F.; Grass, M. E.; Zhang, Y. W.; Butcher, D. R.; Aksoy, F.; Aloni, S.; Altoe, V.; Alayoglu, S.; Renzas, J. R.; Tsung, C. K.; Zhu, Z. W.; Liu, Z.; Salmeron, M.; Somorjai, G. A. Evolution of Structure and Chemistry of Bimetallic Nanoparticle Catalysts under Reaction Conditions. *J. Am. Chem. Soc.* **2010**, *132*, 8697–8703.

(5) Peng, Z. M.; Yang, H. Designer Platinum Nanoparticles: Control of Shape, Composition in Alloy, Nanostructure and Electrocatalytic Property. *Nano Today* **2009**, *4*, 143–164.

(6) Somorjai, G. A.; Frei, H.; Park, J. Y. Advancing the Frontiers in Nanocatalysis, Biointerfaces, and Renewable Energy Conversion by Innovations of Surface Techniques. *J. Am. Chem. Soc.* **2009**, *131*, 16589–16605.

(7) Wagner, F. T.; Lakshmanan, B.; Mathias, M. F. Electrochemistry and the Future of the Automobile. *J. Phys. Chem. Lett.* **2010**, *1*, 2204–2219.

(8) Wang, C.; Daimon, H.; Lee, Y.; Kim, J.; Sun, S. Synthesis of Monodisperse Pt Nanocubes and Their Enhanced Catalysis for Oxygen Reduction. *J. Am. Chem. Soc.* **2007**, *129*, 6974–6975.

(9) Liu, Y. G.; Wang, Y. G.; Zhang, J. Y.; Shi, S. L.; Feng, P.; Wang, T. H. Observation of Surface Structural Changes of Pt Octahedron Nanoparticles and Its Effect in Electrocatalysis Oxidation of Methanol. *Catal. Commun.* **2009**, *10*, 1244–1247.

(10) Tian, N.; Zhou, Z. Y.; Sun, S. G.; Ding, Y.; Wang, Z. L. Synthesis of Tetrahexahedral Platinum Nanocrystals with High-index Facets and High Electro-oxidation Activity. *Science* **2007**, *316*, 732–735.

(11) Yu, T.; Kim, D.; Zhang, H.; Xia, Y. Platinum Concave Nanocubes with High-index Facets and Their Enhanced Activity for Oxygen Reduction Reaction. *Angew. Chem., Int. Ed.* **2011**, *50*, 2773–2777.

(12) Stamenkovic, V. R.; Mun, B. S.; Mayrhofer, K. J. J.; Ross, P. N.; Markovic, N. M.; Rossmeisl, J.; Greeley, J.; Nørskov, J. K. Changing the Activity of Electrocatalysts for Oxygen Reduction by Tuning the Surface Electronic Structure. *Angew. Chem., Int. Ed.* **2006**, *45*, 2897–2901.

(13) Greeley, J.; Stephens, I. E. L.; Bondarenko, A. S.; Johansson, T. P.; Hansen, H. A.; Jaramillo, T. F.; Rossmeisl, J.; Chorkendorff, I.; Nørskov, J. K. Alloys of Platinum and Early Transition Metals as Oxygen Reduction Electrocatalysts. *Nat.Chem.* **2009**, *1*, 552–556.

(14) Lim, B.; Jiang, M.; Camargo, P. H. C.; Cho, E. C.; Tao, J.; Lu, X.; Zhu, Y.; Xia, Y. Pd-Pt Bimetallic Nanodendrites with High Activity for Oxygen Reduction. *Science* **2009**, *324*, 1302–1305.

(15) Stamenkovic, V. R.; Fowler, B.; Mun, B. S.; Wang, G.; Ross, P. N.; Lucas, C. A.; Markovic, N. M. Improved Oxygen Reduction Activity on $Pt_3Ni(111)$ via Increased Surface Site Availability. *Science* **2007**, *315*, 493−497.
(16) Carpenter, M. K.; Moylan, T. E.; Kukreja, R. S.; Atwan, M. H.; Tessema, M. M. Solvothermal Synthesis of Platinum Alloy Nanoparticles for Oxygen Reduction Electrocatalysis. *J. Am. Chem. Soc.* **2012**, *134*, 8535−8542.
(17) Xu, Q.; Chandra, M. Catalytic Activities of Non-noble Metals for Hydrogen Generation from Aqueous Ammonia−Borane at Room Temperature. *J. Power Sources* **2006**, *163*, 364−370.
(18) Yamada, Y.; Yano, K.; Fukuzumi, S. Catalytic Application of Shape-Controlled Cu_2O Particles Protected by Co_3O_4 Nanoparticles for Hydrogen Evolution from Ammonia Borane. *Energy Environ. Sci.* **2012**, *5*, 5356−5363.
(19) Yan, J. M.; Zhang, X. B.; Han, S.; Shioyama, H.; Xu, Q. Iron-nanoparticle Catalyzed Hydrolytic Dehydrogenation of Ammonia Borane for Chemical Hydrogen Storage. *Angew. Chem., Int. Ed.* **2008**, *47*, 2287−2289.
(20) Metin, Ö.; Mazumder, V.; Özkar, S.; Sun, S. Monodisperse Nickel Nanoparticles and Their Catalysis in Hydrolytic Dehydrogenation of Ammonia Borane. *J. Am. Chem. Soc.* **2010**, *132*, 1468−1469.
(21) Li, Y. Q.; Xie, L.; Liu, Y.; Yang, R.; Li, X. G. Favorable Hydrogen Storage Properties of M (HBTC)(4,4′-bipy)·3DMF (M = Ni and Co). *Inorg. Chem.* **2008**, *47*, 10372−10377.
(22) Bertolini, J. C. Local Order at the Surface of Binary Alloys in Relation to Their Chemical Reactivity. *Surf. Rev. Lett.* **1996**, *3*, 1857−1868.
(23) Markovic, N. M.; Gasteiger, H. A.; Ross, P. N.; Jiang, X.; Villegas, I.; Weaver, M. J. Electrooxidation Mechanisms of Methanol and Formic-acid on Pt-Ru Alloy Surfaces. *Electrochim. Acta* **1995**, *40*, 91−98.
(24) Gojkovic, S. L.; Vidakovic, T. R.; Durovic, D. R. Kinetic Study of Methanol Oxidation on Carbon-Supported Pt-Ru Electrocatalyst. *Electrochim. Acta* **2003**, *48*, 3607−3614.
(25) Hu, Y.; Wu, P.; Yin, Y.; Zhang, H.; Cai, C. Effects of Structure, Composition, and Carbon Support Properties on the Electrocatalytic Activity of Pt-Ni-graphene Nanocatalysts for the Methanol Oxidation. *Appl. Catal., B* **2012**, *111*, 208−217.
(26) Chen, C.; Pan, F.; Yu, H. Electrocatalytic Activity of Pt Nanoparticles on A Karst-like Ni Thin Film toward Methanol Oxidation in Alkaline Solutions. *Appl. Catal., B* **2011**, *104*, 382−389.
(27) Papadimitriou, S.; Armyanov, S.; Valova, E.; Hubin, A.; Steenhaut, O.; Pavlidou, E.; Kokkinidis, G.; Sotiropoulos, S. Methanol Oxidation at Pt-Cu, Pt-Ni, and Pt-Co Electrode Coatings Prepared by a Galvanic Replacement Process. *J. Phys. Chem. C* **2010**, *114*, 5217−5223.
(28) Sun, S.; Murray, C. B.; Weller, D.; Folks, L.; Moser, A. Monodisperse FePt Nanoparticles and Ferromagnetic FePt Nanocrystal Superlattices. *Science* **2000**, *287*, 1989−1992.
(29) Kim, J.; Rong, C.; Liu, J. P.; Sun, S. Dispersible Ferromagnetic FePt Nanoparticles. *Adv. Mater.* **2009**, *21*, 906−909.
(30) Wang, C.; Hou, Y.; Kim, J.; Sun, S. A General Strategy for Synthesizing FePt Nanowires and Nanorods. *Angew. Chem., Int. Ed.* **2007**, *46*, 6333−6335.
(31) Harpeness, R.; Gedanken, A. The Microwave-Assisted Polyol Synthesis of Nanosized Hard Magnetic Material, FePt. *J. Mater. Chem.* **2005**, *15*, 698−702.
(32) Nakaya, M.; Tsuchiya, Y.; Ito, K.; Oumi, Y.; Sano, T.; Teranishi, T. Novel Synthesis of FePt Nanoparticles and Magnetic Properties of Their Self-Assembled Superlattices. *Chem. Lett.* **2004**, *33*, 130−131.
(33) Wu, B.; Zheng, N.; Fu, G. Small Molecules Control the Formation of Pt Nanocrystals: A Key Role of Carbon Monoxide in the Synthesis of Pt Nanocubes. *Chem. Commun.* **2011**, *47*, 1039−1041.
(34) Gibot, P.; Tronc, E.; Chaneac, C.; Jolivet, J. P.; Fiorani, D.; Testa, A. M. (Co, Fe) Pt Nanoparticles by Aqueous Route; Self-Assembling, Thermal and Magnetic Properties. *J. Magn. Magn. Mater.* **2005**, *290*, 555−558.
(35) Yang, X. J.; Cheng, F. Y.; Liang, J.; Tao, Z. L.; Chen, J. Pt_xNi_{1-x} Nanoparticles as Catalysts for Hydrogen Generation from Hydrolysis of Ammonia Borane. *Int. J. Hydrogen Energy* **2009**, *34*, 8785−8791.
(36) Gutowska, A.; Li, L. Y.; Shin, Y. S.; Wang, C. M. M.; Li, X. H. S.; Linehan, J. C.; Smith, R. S.; Kay, B. D.; Schmid, B.; Shaw, W.; Gutowski, M.; Autrey, T. Nanoscaffold Mediates Hydrogen Release and the Reactivity of Ammonia Borane. *Angew. Chem., Int. Ed.* **2005**, *44*, 3578−3582.
(37) Chen, Y. S.; Fulton, J. L.; Linehan, J. C.; Autrey, T. In Situ XAFS and NMR Study of Rhodium-Catalyzed Dehydrogenation of Dimethylamineborane. *J. Am. Chem. Soc.* **2005**, *127*, 3254−3255.
(38) Sit, V.; Geanangel, R. A.; Wendlandt, W. W. The Thermal Dissociation of NH_3BH_3. *Thermochim. Acta* **1987**, *113*, 379−382.
(39) Chandra, M.; Xu, Q. A High-performance Hydrogen Generation System: Transition Metal-Catalyzed Dissociation and Hydrolysis of Ammonia-Borane. *J. Power Sources* **2006**, *156*, 190−194.
(40) Chen, W.; Ji, J.; Duan, X.; Qian, G.; Li, P.; Zhou, X.; Chen, D.; Yuan, W. Unique Reactivity in Pt/CNT Catalyzed Hydrolytic Dehydrogenation of Ammonia Borane. *Chem. Commun.* **2014**, *50*, 2142−2144.
(41) Bao, H. L.; Li, J.; Jiang, L. H.; Shang, M. F.; Zhang, S.; Jiang, Z.; Wei, X. J.; Huang, Y. Y.; Sun, G. Q.; Wang, J. Q. Structure of Pt_nNi Nanoparticles Electrocatalysts Investigated by X-ray Absorption Spectroscopy. *J. Phys. Chem. C* **2013**, *117*, 20584−20591.
(42) Nassr, A. B. A. A.; Sinev, I.; Grünert, W.; Bron, M. PtNi Supported on Oxygen Functionalized Carbon Nanotubes: In Depth Structural Characterization and Activity for Methanol Electrooxidation. *Appl. Catal., B* **2013**, *142*−*143*, 849−860.
(43) Tupy, S. A.; Karim, A. M.; Bagia, C.; Deng, W. H.; Huang, Y. L.; Vlachos, D. G.; Chen, J. G. Correlating Ethylene Glycol Reforming Activity with in situ EXAFS Detection of Ni Segregation in Supported NiPt Bimetallic Catalysts. *ACS Catal.* **2012**, *2*, 2290−2296.
(44) Teliska, M.; Murthi, V. S.; Mukerjee, S.; Ramaker, D. E. Correlation of Water Activation, Surface Properties, and Oxygen Reduction Reactivity of Supported Pt-M/C Bimetallic Electrocatalysts Using XAS. *J. Electrochem. Soc.* **2005**, *152*, A2159−A2169.
(45) Lai, F.; Sarma, L. S.; Chou, H.; Liu, D.; Hsieh, C. A.; Lee, J. F.; Hwang, B. J. Architecture of Bimetallic Pt_xCo_{1-x} Electrocatalysts for Oxygen Reduction Reaction as Investigated by X-ray Absorption Spectroscopy. *J. Phys. Chem. C* **2009**, *113*, 12674−12681.
(46) Lu, P.; Teranishi, T.; Asakura, K.; Miyake, M.; Toshima, N. Polymer-Protected Ni/Pd Bimetallic Nano-clusters: Preparation, Characterization and Catalysis for Hydrogenation of Nitrobenzene. *J. Phys. Chem. B* **1999**, *103*, 9673−9682.
(47) Xiao, L.; Wang, L. Structures of Platinum Clusters: Planar or Spherical? *J. Phys. Chem. A* **2004**, *108*, 8605−8614.